Rotationally resolved photoelectron spectroscopic study of the Jahn–Teller effect in allene

Author(s):
Schulenburg, A.M.; Merkt, Frédéric

Publication date:
2009-01-21

Permanent link:
https://doi.org/10.3929/ethz-a-010800521

Originally published in:
The Journal of Chemical Physics 130(3), https://doi.org/10.1063/1.3056385

The following article appeared in *J. Chem. Phys.* **130**, 034308 (2009) and may be found at http://dx.doi.org/10.1063/1.3056385.

Rotationally resolved photoelectron spectroscopic study of the Jahn–Teller effect in allene

A. M. Schulenburg and F. Merkt

Citation: J. Chem. Phys. **130**, 034308 (2009); doi: 10.1063/1.3056385
View online: http://dx.doi.org/10.1063/1.3056385
View Table of Contents: http://aip.scitation.org/toc/jcp/130/3
Published by the American Institute of Physics

Rotationally resolved photoelectron spectroscopic study of the Jahn–Teller effect in allene

A. M. Schulenburg and F. Merkt[a)]
Laboratorium für Physikalische Chemie, ETH Zürich, CH-8092 Zürich, Switzerland

(Received 31 October 2008; accepted 2 December 2008; published online 21 January 2009)

The pulsed-field-ionization zero-kinetic-energy photoelectron spectra of allene (C_3H_4) and perdeuterated allene have been recorded from the first adiabatic ionization energy up to 2200 cm^{-1} of internal energy in the cations at a resolution sufficient to observe the full rotational structure. The intensity distributions in the spectra are dominated by vibrational progressions in the torsional mode, which were analyzed in the realm of a two-dimensional model of the $E\otimes(b_1\oplus b_2)$ Jahn–Teller effect in the allene cation [C. Woywod and W. Domcke, Chem. Phys. **162**, 349 (1992)]. Whereas the rotational structure of the transitions to the lowest torsional levels (0^0 and 4^1) are regular and can be qualitatively analyzed in terms of a simple orbital ionization model, the rotational structure of the spectra of the 4^2 and 4^3 levels are strongly perturbed. The photoelectron spectrum of C_3H_4 also reveals several weak vibrational bands in the immediate vicinity of these levels that are indicative of (ro)vibronic perturbations. A slight broadening of the transitions to the 4^1 levels compared to that of the vibronic ground state and the increase of the number of sharp features in the rotational structure of the spectrum of the 4^2 level point at the importance of large-amplitude motions not considered in previous treatments of the Jahn–Teller effect in the allene cation. © *2009 American Institute of Physics*. [DOI: 10.1063/1.3056385]

I. INTRODUCTION

Allene has been the object of much investigation for its relevance to astrochemistry[1–3] and to studies of photodissociation dynamics.[4–9] Allene is also the smallest member of the cumulene family and one of the simplest representatives of the $D_{2d}(M)$ molecular symmetry group. The $\tilde{X}^+\,^2E$ electronic ground state of the cation exhibits the $E\otimes(b_1\oplus b_2)$ Jahn–Teller (JT) effect[10,11] encountered only in molecules with one or more $4n$-fold axes of symmetry: A strong distortion along the torsional mode ν_4 (b_1 symmetry) is revealed in the He I photoelectron spectrum by a long progression in that mode.[12–17] Domcke and co-workers[18,19] successfully analyzed the vibronic structure of the He I photoelectron spectra with the aid of JT coupling parameters calculated *ab initio* and a vibronic JT Hamiltonian. They determined the C=C=C asymmetric stretching mode ν_6 of b_2 symmetry to be the other main JT active mode.

The present work aimed at resolving the rotational structure in the photoelectron spectrum of allene and allene-d_4 with up to 2200 cm^{-1} of internal excitation of the cations and at obtaining previously unobserved details of its vibronic structure at low energies to characterize the $E\otimes(b_1\oplus b_2)$ JT effect in the allene cation. High-resolution pulsed-field-ionization zero-kinetic-energy (PFI-ZEKE) photoelectron spectroscopic experiments enabled a resolution of up to 0.15 cm^{-1} for single rovibronic transitions.

II. EXPERIMENTAL

Two different laser systems described in Refs. 20 and 21 have been employed in the study of the rovibronic structure of the photoelectron spectrum of allene: A broadly tunable vacuum-ultraviolet (vuv) laser system[20] with a bandwidth of 0.1 cm^{-1} was employed to obtain an overview of the PFI-ZEKE photoelectron spectrum over a range of nearly 2500 cm^{-1} with partial rotational resolution. A high-resolution vuv laser system[21] with a Fourier-transform-limited bandwidth of 0.008 cm^{-1} was used to resolve the full rotational structure of selected bands of the photoelectron spectrum. The vuv radiation was generated by resonance-enhanced four-wave mixing ($\tilde{\nu}_{vuv}=2\tilde{\nu}_1-\tilde{\nu}_2$) using the $(4p)^5(^2P_{3/2})5p[1/2](J=0)\leftarrow(4p)^6\,^1S_0$ two-photon resonance in krypton at $2\tilde{\nu}_1=94\,092.862$ cm^{-1}.[22,23] The setup used in the four-wave mixing is described in Ref. 24.

Allene-d_4 was synthesized according to the method of Morse and Leitch[25] by the reaction of hexachloropropene with deuterium oxide and zinc. The by-product propyne-d_4 was removed from the reaction product by Mayers reagent [mercury(II) chloride—potassium iodide solution]. The yield of allene-d_4 was 50% with a deuterium content of at least 96% and a purity of 94% with 2% propene-d_6 and 4% propyne-d_4 as the main impurities.

Mixtures of 500 mbar allene (allene-h_4: Aldrich, purity 97%; allene-d_4: as described above) in 5 bar Ar at a total stagnation pressure of about 2–3 bar were introduced into the chamber through a pulsed nozzle (General Valve) and cooled to a rotational temperature of ≈10 K in a supersonic jet expansion into the high vacuum. The molecular beam was skimmed and subsequently intersected the vuv laser beam at right angles in the photoionization region.[20]

The overview PFI-ZEKE photoelectron spectra were recorded with a simple two-pulse electric field sequence. A "discrimination" pulse of +105 mV/cm and 1 μs duration

[a)]Electronic mail: feme@xuv.phys.chem.ethz.ch.

was applied 3 μs after photoexcitation to remove electrons formed by direct ionization and was immediately followed by an "extraction" pulse of −140 mV/cm. To achieve nearly fully rotationally resolved photoelectron spectra, the narrow-bandwidth laser system[21] was used in combination with a multipulse electric field sequence[26,27] delayed by 1.7 μs relative to the time of photoexcitation and optimized to field-ionize narrow slices of the pseudocontinuum of high-n Rydberg states below each ionization threshold. A discrimination pulse of +172 mV/cm was applied for 1 μs, followed immediately by stepwise increasing extraction pulses of −86, −129, −172, −215, −259, −302, and −345 mV/cm, each step being 300 ns long. Electrons field ionized by each of the extraction pulses were monitored according to their different extraction times and therefore different arrival times on a microchannel plate detector. The best compromise between high resolution and signal-to-noise ratio was achieved by monitoring the electrons extracted by the pulse of −172 mV/cm, resulting in a full width at half maximum (FWHM) of 0.15 cm^{-1} for lines corresponding to a single transition. A correction of +1.6(2) cm^{-1} was introduced to account for the shifts of the rovibronic ionization thresholds induced by the −172 mV/cm step of the electric field pulse sequence.[26]

III. THE VIBRONIC STRUCTURE IN THE PFI-ZEKE PHOTOELECTRON SPECTRA OF C_3H_4 AND C_3D_4

Ground state neutral allene has a D_{2d} equilibrium geometry. The allene cation possesses a doubly degenerate ^2E ground state at the D_{2d} equilibrium geometry of the neutral and is thus subject to a JT distortion. The vibrational modes that can couple the two E components of the electronic state in first order must be of an irreducible representation that is contained in the direct product formed by the two E components of the electronic state:

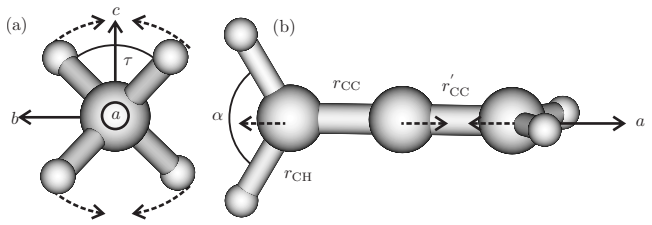

FIG. 1. Schematic representation of (a) the torsional and (b) the asymmetric C=C=C stretching mode of allene. The motion of the atoms is indicated by the dashed arrows. The internal coordinates and the inertial axes (full arrows) are also indicated.

$$E \otimes E = a_1 \oplus [a_2] \oplus b_1 \oplus b_2, \tag{1}$$

thus rendering all nondegenerate vibrational degrees of freedom of allene JT active. There are no vibrational modes of a_2 symmetry and a_1 modes do not lead to distortions of the geometry of the cation away from the symmetric configuration so that the resulting JT effect is denoted $E \otimes (b_1 \oplus b_2)$, the capital E representing the electronic symmetry label and the lower case letters b_1 and b_2 the symmetry labels of the JT active modes. The allene cation in its D_{2d} structure has three modes of b_2 symmetry and one of b_1 symmetry. The torsional mode ν_4 of b_1 symmetry and the C=C=C asymmetric stretching mode ν_6 of b_2 symmetry were identified as causing the greatest stabilization of the molecular cation of allene by *ab initio* calculations.[19] The two vibrational modes ν_4 and ν_6 are depicted schematically in Figs. 1(a) and 1(b), respectively, where the inertial axis system and internal coordinates are also indicated. Quadratic and bilinear JT coupling parameters have not been determined to date, and we will limit the discussion here to the linear $E \otimes (b_1 \oplus b_2)$ JT effect in allene. Restricting the treatment to only the two strongly JT active modes (ν_4 and ν_6), the Hamiltonian matrix $\mathbf{H}$ for the electronic part of the $E \otimes (b_1 \oplus b_2)$ JT problem is expressed in the diabatic basis of the two components of the electronic ^2E state as[19]

$$\mathbf{H} = \left[E_0 \mathbf{1} + \underbrace{\sum_{i=1}^{15} \begin{pmatrix} \hat{T}_i + \frac{1}{2}\tilde{\nu}_i q_i^2 & 0 \\ 0 & \hat{T}_i + \frac{1}{2}\tilde{\nu}_i q_i^2 \end{pmatrix}}_{\mathbf{H}_{\text{h.o.}}} + \underbrace{\begin{pmatrix} k_6 q_6 & k_4 q_4 \\ k_4 q_4 & -k_6 q_6 \end{pmatrix}}_{\mathbf{H}_{\text{JT}}} \right], \tag{2}$$

where $\mathbf{1}$ is the $2 \otimes 2$ unit matrix and $\hat{T}_i$ represents the kinetic energy operator along the dimensionless normal coordinate q_i. The position of the conical intersection above the neutral rovibronic ground state E_0, the vibrational harmonic wave numbers $\tilde{\nu}_i$ and the linear JT coupling parameters $k_{i=4,6}$ are expressed in units of cm^{-1}. The corresponding two-dimensional potential energy surface of the allene cation is depicted schematically in Fig. 2. The minima of the potential energy hypersurface $V_{\min,i}$ along q_6 ($q_{i\neq 6}=0$) and q_4 ($q_{i\neq 4}=0$) of the lower adiabatic potential energy sheet lie

$$V_{\min,i} = -\frac{k_i^2}{2\tilde{\nu}_i}, \quad i = 4,6 \tag{3}$$

below the conical intersection at E_0. Using the coupling constants and harmonic wave numbers determined from values initially estimated by *ab initio* calculations and subsequently

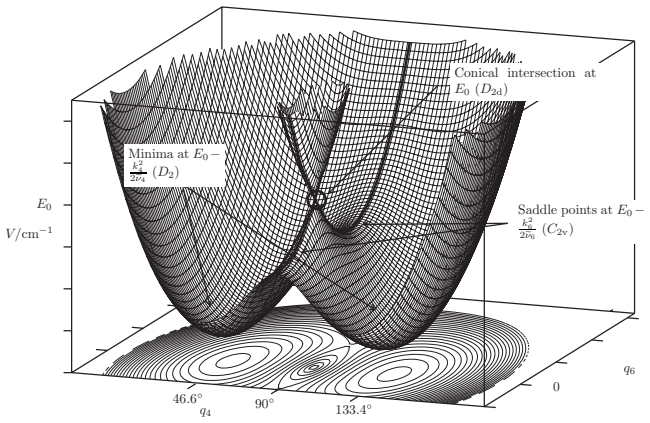

FIG. 2. Cut through the potential energy hypersurface of $C_3H_4^+$ along the torsional mode q_4 and the asymmetric C=C=C stretching mode q_6. The two minima correspond to a D_2 geometry in agreement with previous work that found the equivalent minimum energy structure to have torsional angles of 46.6° and 133.4° and $r_{CC}=r'_{CC}$ (Ref. 19). The structure of $C_3H_4^+$ at the saddle points located at a torsional angle of 90° and $r_{CC}\neq r'_{CC}$ is of C_{2v} symmetry. A contour diagram of the two-dimensional potential energy surface along q_4 and q_6 is also displayed.

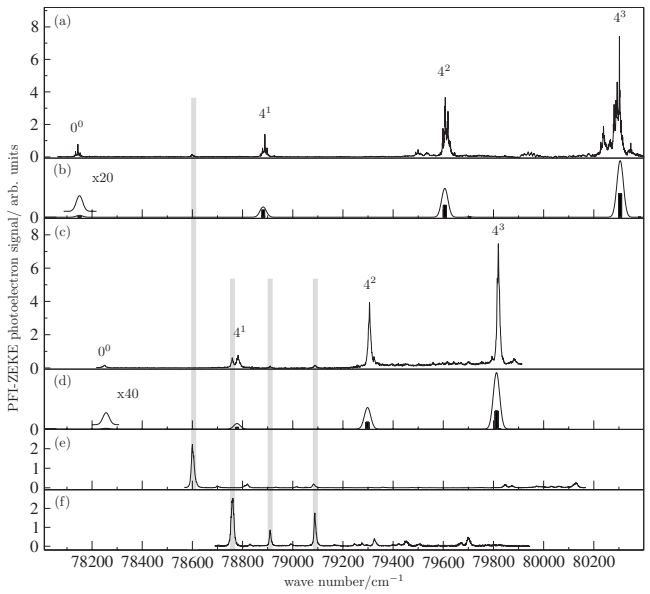

FIG. 3. PFI-ZEKE photoelectron spectra of (a) C_3H_4, (c) C_3D_4, (e) C_3H_6 and (f) C_3D_6. The progressions observed in (a) and (c) are assigned to the torsional mode ν_4 and labeled in the notation 4^{v_4}. Vibronic bands originating from C_3H_6 and C_3D_6 are highlighted by gray bars. Panels (b) and (d) show the calculations of the vibronic structure based on Eq. (2) and the linear JT coupling parameters and wave numbers reported in Ref. 19.

fitted to an experimental He I spectrum[19] (tabulated in Table I), two minima along q_4 located 4140 cm^{-1} below the D_{2d} conical intersection are obtained from Eq. (3). At the minimum geometry the torsional angle is reduced ($\tau=46.6°$) and both C=C bond lengths are equal.[19] The two saddle points along q_6 have C_{2v} symmetry and are located 1334 cm^{-1} below the conical intersection. The four CH bonds r_{CH} are of equal length and the two H–C–H angles α are equal (the internal coordinates of allene are defined in Fig. 1). Unlike in the $E\otimes e$ JT effect, typical for molecules with an odd-fold symmetry axis for which an isoenergetic circular path around the conical intersection results from linear JT coupling,[28,29,11] the minimum energy path around the conical intersection in the $E\otimes(b_1\oplus b_2)$ JT effect has two minima and two maxima (corresponding to the saddle points of C_{2v} geometry in Fig. 2) at $q_6=0$ and $q_4=0$, respectively (or vice versa) because the harmonic wave numbers and coupling constants of the JT active modes of b_1 and b_2 symmetries are different. The saddle points on the two-dimensional surfaces separate the two minima of D_2 symmetry by a barrier of 2806 cm^{-1}.[19] The geometry at the saddle points has been estimated to have a torsional angle $\tau=90°$, and C=C bond lengths of $r_{CC}\approx 1.34$ Å and $r'_{CC}\approx 1.44$ Å.[30]

The overview PFI-ZEKE photoelectron spectra of the $\tilde{X}^+\,^2E\leftarrow\tilde{X}\,^1A_1$ photoionizing transition of allene and allene-d_4 are displayed in panels (a) and (c) of Fig. 3, respectively. The spectra exhibit a progression of regularly spaced bands of uniformly increasing intensity separated by ≈746 and ≈532 cm^{-1}, respectively. These progressions are interpreted as vibrational progressions in the torsional mode.[16] Each band of the progression is assigned to a torsional level of the cation in the usual notation 4^{v_4}.[31] The central positions of the vibronic bands observed in the PFI-ZEKE photoelectron spectra of allene and allene-d_4 are summarized in Table II. The gray vertical bars in Fig. 3 mark transitions that originate from small amounts of propene and propene-d_6 in the samples of allene and allene-d_4, respectively. These impurity lines were identified in separate measurements of the PFI-ZEKE photoelectron spectra of propene and propene-d_6, which are displayed in Figs. 3(e) and 3(f), respectively. Although these impurity lines have been observed in previous He I photoelectron spectroscopic studies,[16,17] they have never been identified as such.

The vibrational progression in the PFI-ZEKE photoelectron spectra is a clear indication of the cation being distorted along the torsional mode ν_4 relative to the neutral ground state [see Fig. 1(a)]. Although the C=C=C asymmetric

TABLE I. Coupling constants, vibrational harmonic wave numbers of the main JT active modes and JT stabilization energies for the $\tilde{X}^+\,^2E$ ground state of $C_3H_4^+$ and $C_3D_4^+$.

	$\tilde{\nu}_{i,\mathrm{H}}$ [a]	$k_{i,\mathrm{H}}$ [a]	$V_{\mathrm{min},i}$	$\tilde{\nu}_{i,\mathrm{D}}$	$k_{i,\mathrm{D}}$	$V_{\mathrm{min},i}$	$\frac{\tilde{\nu}_{i,\mathrm{D}}^{\mathrm{neutral}}}{\tilde{\nu}_{i,\mathrm{H}}^{\mathrm{neutral}}}$
ν_4	750 cm^{-1}	2492 cm^{-1}	−4140 cm^{-1}	534 cm^{-1}	2102 cm^{-1}	−4140 cm^{-1}	0.7113[b]
ν_6	1912 cm^{-1}	2258 cm^{-1}	−1334 cm^{-1}	1873 cm^{-1}	2236 cm^{-1}	−1334 cm^{-1}	0.9800[c]

[a]From Ref. 19. The values have been converted to cm^{-1} using the relation 1 eV=8065.544 cm^{-1}.
[b]From Refs. 39 and 40.
[c]From Refs. 41 and 42.

TABLE II. Positions relative to the adiabatic ionization energy of all vibronic bands observed in the PFI-ZEKE photoelectron spectra of C_3H_4 and C_3D_4 labeled as in Figs. 3 and 8. Numbers in parentheses correspond to the uncertainties in the determination of the band centers in units of the last figure.

	$E_{obs}-E_i$ (cm^{-1})	
Label	$C_3H_4^+$	$C_3D_4^+$
0^0	0.0	0.0
4^1	745.7(7)	532(2)
I	1358(5)	⋯
II	1391(7)	⋯
III	1420(15)	⋯
4^2	1465(12)	1057(3)
IV (6^1) [a]	1543(5)	⋯
V	2096(10)	⋯
VI	2122(10)	⋯
4^3	2150(15)	1570(3)
VII (4^16^1?)	2205(15)	⋯
4^4	⋯	2086(5)[b]

[a] $A^+=4.75(8)$ cm^{-1} is estimated from the Q-type branches.
[b] Not displayed in Fig. 3.

stretch ν_6 of b_2 symmetry represents a second strongly JT active mode,[19] the photoelectron spectrum does not reveal strong spectral features that could be attributed to this mode. Only the 6^1 asymmetric C=C=C stretching level is expected to be observable in the energy region above the adiabatic ionization threshold studied here because of the high value of the harmonic wave number ($\tilde{\nu}_6=1911$ cm^{-1}). However, the distortion along ν_6 is less than along ν_4 and the intensity of the transition to the 6^1 level of the cation is not expected to be as strong as the transition to the fundamental of the torsion. This qualitative argument is confirmed by a more rigorous treatment of the JT effect (see Sec. V and Fig. 8 below, and Refs. 18 and 19).

The Franck–Condon factors can be estimated by considering the minimum energy structures of the neutral and cationic states and approximating the vibrational wave functions by harmonic oscillator wave functions in the corresponding potential energy wells. By virtue of symmetry, there is no tunneling between the potential energy wells of D_2 geometry through a structure with $\tau=90°$, even for vibrational levels located close to the conical intersection. In D_2 symmetry, all vibrational levels of the torsional mode transform as the totally symmetric representation a_1, and a smooth intensity distribution is expected.

In panels (b) and (d) of Fig. 3, the vibronic positions and intensity distributions calculated on the basis of the JT Hamiltonian of Eq. (2) are displayed as stick spectra. The panels also show synthetic spectra obtained after convolution with a Gaussian instrumental function with a FWHM of 20 cm^{-1}. The linear JT coupling constants $k_{i,H}$ and vibrational frequencies $\tilde{\nu}_{i,H}$ of $C_3H_4^+$ were taken from Ref. 19 (see Table I). The linear JT coupling parameter $k_{i,D}$ and the harmonic wave number $\tilde{\nu}_{i,D}$ for the torsion and asymmetric C=C=C stretch for $C_3D_4^+$ can be determined from those of $C_3H_4^+$ by appropriate mass scaling. Assuming the structure of the cation at the conical intersection to be that of the neutral, one obtains from the vibronic wave numbers $\tilde{\nu}_{i,H(D)}^{neutral}$ for C_3H_4 (C_3D_4) and $\tilde{\nu}_{i,H(D)}$ for $C_3H_4^+$ ($C_3D_4^+$),

$$\tilde{\nu}_{i,D}=\frac{\tilde{\nu}_{i,D}^{neutral}}{\tilde{\nu}_{i,H}^{neutral}}\cdot\tilde{\nu}_{i,H}. \tag{4}$$

In first approximation, the stabilization energy of the JT problem does not depend on the deuteration of the system as it is a purely electronic property of the system, i.e., $V_{min,i}^{H}=V_{min,i}^{D}$. Neglecting zero-point energy corrections, the following relationship between the linear JT coupling constants of the per- and undeuterated species can be obtained from Eq. (3):

$$k_{i,D}=k_{i,H}\cdot\sqrt{\frac{\tilde{\nu}_{i,D}}{\tilde{\nu}_{i,H}}}. \tag{5}$$

The linear JT coupling constants and the harmonic wave numbers for $C_3D_4^+$ are summarized in the lower half of Table I. To calculate the line positions in the photoelectron spectrum the vibronic wave functions ψ_{ve} were represented as products of the vibrational harmonic oscillator wave functions $|v_6,v_4\rangle$ of the JT active modes with the degenerate components of the electronic wave function $|\Lambda\rangle$,

$$\psi_{ve}=|v_6,v_4,\Lambda\rangle=|v_6,v_4\rangle|\Lambda\rangle, \tag{6}$$

where Λ is the projection of the electronic angular momentum onto the principal axis (a-axis, see Fig. 1) and takes the values +1 and −1 for a doubly degenerate state. The JT Hamiltonian of Eq. (2) was expressed in the harmonic basis of ν_4 and ν_6 [Eq. (6)], as described in Refs. 19 and 28, truncating the basis set at values of $v_4\leq 34$ and $v_6\leq 34$ so that the lowest eigenvalues obtained had converged within 0.1 cm^{-1}. Diagonalization of the JT Hamiltonian in the basis of the JT active modes yielded two perfectly degenerate eigenfunctions for each vibronic level i,

$$\psi_+^i=\sum_{v_4+v_6=\text{even}}c_{v_4,v_6}^i|v_4,v_6\rangle|\Lambda=+1\rangle+\sum_{v_4+v_6=\text{odd}}c_{v_4,v_6}^i|v_4,v_6\rangle|\Lambda=-1\rangle, \tag{7}$$

$$\psi_-^i=\sum_{v_4+v_6=\text{odd}}c_{v_4,v_6}^i|v_4,v_6\rangle|\Lambda=+1\rangle+\sum_{v_4+v_6=\text{even}}c_{v_4,v_6}^i|v_4,v_6\rangle|\Lambda=-1\rangle, \tag{8}$$

where $c_{k,l}^i$ are expansion coefficients. No attempt to fit the JT parameters or harmonic wave numbers was attempted because of the small numbers of vibronic bands observed in the spectra and the excellent agreement with experimental results that could be reached with the parameters in Ref. 19.

The intensities I_i of the transitions to the final states v_i from the $\tilde{X}^+\,{}^1A_1(0^0)$ initial vibronic state were estimated as being proportional to the squares of the coefficients $c_{0,0}^i$ of the wave functions,

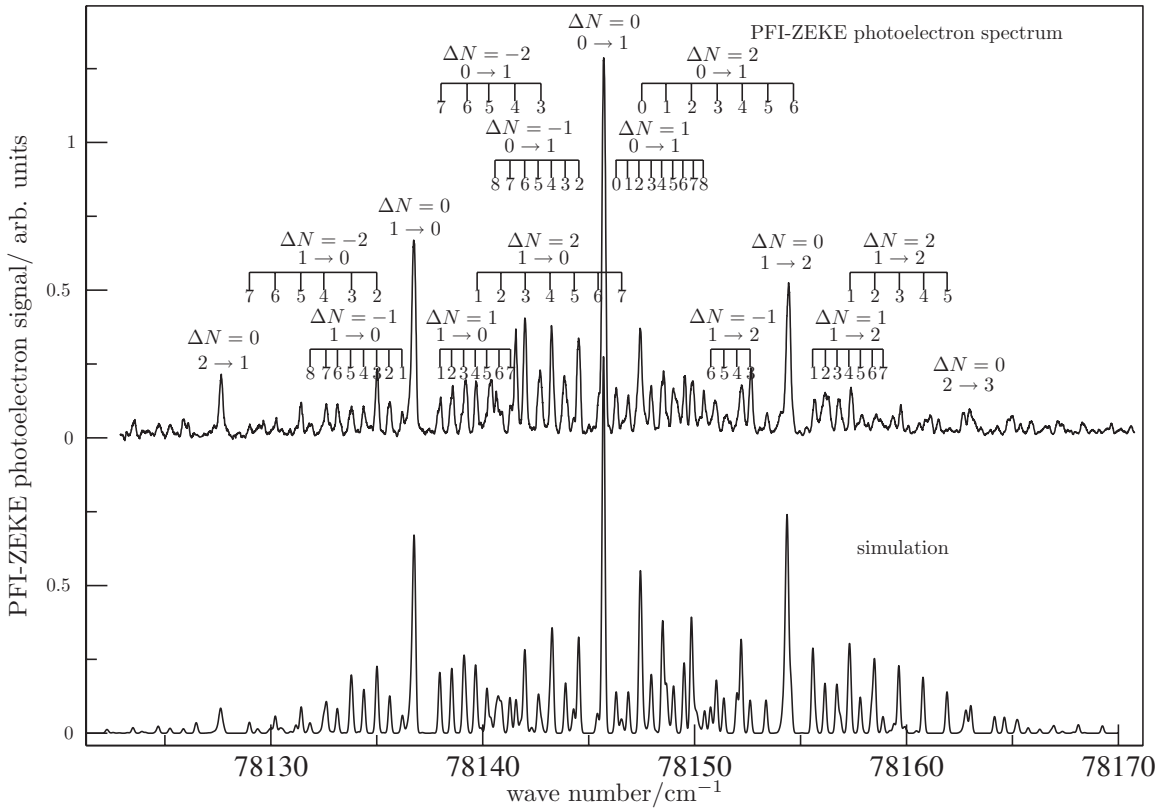

FIG. 4. Upper panel: PFI-ZEKE photoelectron spectrum of the origin band of the $\tilde{X}^+\,^2E \leftarrow \tilde{X}\,^1A_1$ transition of C_3H_4. Lower trace: simulated spectrum using a Gaussian instrument function of FWHM of 0.15 cm^{-1}. The assignment bars are grouped according to the change in the total angular momentum ΔN and the change in K_a in the notation $K_a'' \rightarrow K_a^+$. Each transition is labeled by the total angular momentum quantum number N'' of the neutral ground state.

$$I_i \propto |c_{0,0}^i|^2, \tag{9}$$

which approximates the Franck–Condon integrals between the vibronic ground state wave function of the neutral and the vibronic wave functions of the cation. The excellent agreement of the vibronic structure of the low-resolution PFI-ZEKE photoelectron spectrum of allene (see Fig. 3) with the vibronic structure calculated using the JT coupling parameters reported in Ref. 19 suggests that these parameters are adequate to describe the JT effect in allene at low resolution. The comparison also indicates that the lowest vibrational levels of the allene cation can be described adequately by assuming that the cation has a D_2 equilibrium structure and is not subject to tunneling between equivalent minima. The high-resolution PFI-ZEKE photoelectron spectra presented in Secs. IV and V, however, provide a more complete picture of the structure and dynamics of the allene cation.

IV. THE ROTATIONAL STRUCTURE OF THE 0^0 AND 4^1 BANDS

The PFI-ZEKE photoelectron spectra of the lowest two members of the torsional progression $(\tilde{X}^+\,^2E(0^0,4^1) \leftarrow \tilde{X}\,^1A_1)$ were recorded at high resolution with the laser system described in Ref. 21. The spectra of the origin (0^0) and the torsional fundamental (4^1) bands are shown in Figs. 4 and 5, respectively. They show sharp rotational lines with FWHMs of 0.15 cm^{-1} in the case of the origin band and 0.2 cm^{-1} in the case of the 4^1 band for single transitions. The simulations of these spectra based on the rovibronic photoionization selection rules presented in Ref. 32 and the orbital ionization model described in Ref. 33 are displayed for comparison below the experimental spectra. Both bands exhibit a similar rotational structure with three strong peaks and weaker but sharp structures between them.

Even in the case of a significant JT distortion along the torsional coordinate, the rotational energy level structures of the $\tilde{X}^+\,^2E$ $(0^0$ and $4^1)$ levels of $C_3H_4^+$ are not expected to deviate strongly from those of a prolate symmetric top, the B^+ and C^+ constants being almost identical ($\simeq$0.3 cm^{-1}) for all torsional angles and much smaller than the A^+ rotational constant ($\simeq$4.7 cm^{-1}).

The symmetry selection rules for the $\tilde{X}^+ \leftarrow \tilde{X}$ ionizing transition of allene are derived according to[32]

$$\Gamma_{\mathrm{rve}} \otimes \Gamma_{\mathrm{rve}}^+ \supseteq (\Gamma^*)^{\ell+1}, \tag{10}$$

where ℓ is the angular momentum quantum number of the outgoing photoelectron partial wave. Γ_{rve} $(\Gamma_{\mathrm{rve}}^+)$ represents the irreducible representation of the rovibronic state of the neutral (cation) and Γ^* the dipole–moment representation.[34] In the $D_2(M)$ molecular symmetry group, Eq. (10) can be expressed in the notation $\Gamma_{\mathrm{rve}}^+ \leftrightarrow \Gamma_{\mathrm{rve}}''$ as

$$A_1 \leftrightarrow A_1, \quad B_1 \leftrightarrow B_1, \quad B_2 \leftrightarrow B_2, \quad B_3 \leftrightarrow B_3, \tag{11}$$

which translates into $\Delta K_a = K_a^+ - K_a'' = \mathrm{odd}$, $\Delta K_c = K_c^+ - K_c'' = \mathrm{odd}$ for transitions from the vibronic ground state of allene to the 0^0 $(\Gamma_{\mathrm{ve}}^+ = B_2)$ (in D_2) and 4^1 $(\Gamma_{\mathrm{ve}}^+ = B_2)$ (in D_2) vibronic levels of the cation. The rovibronic symmetry selection rules do not depend on the parity of the outgoing photoelectron

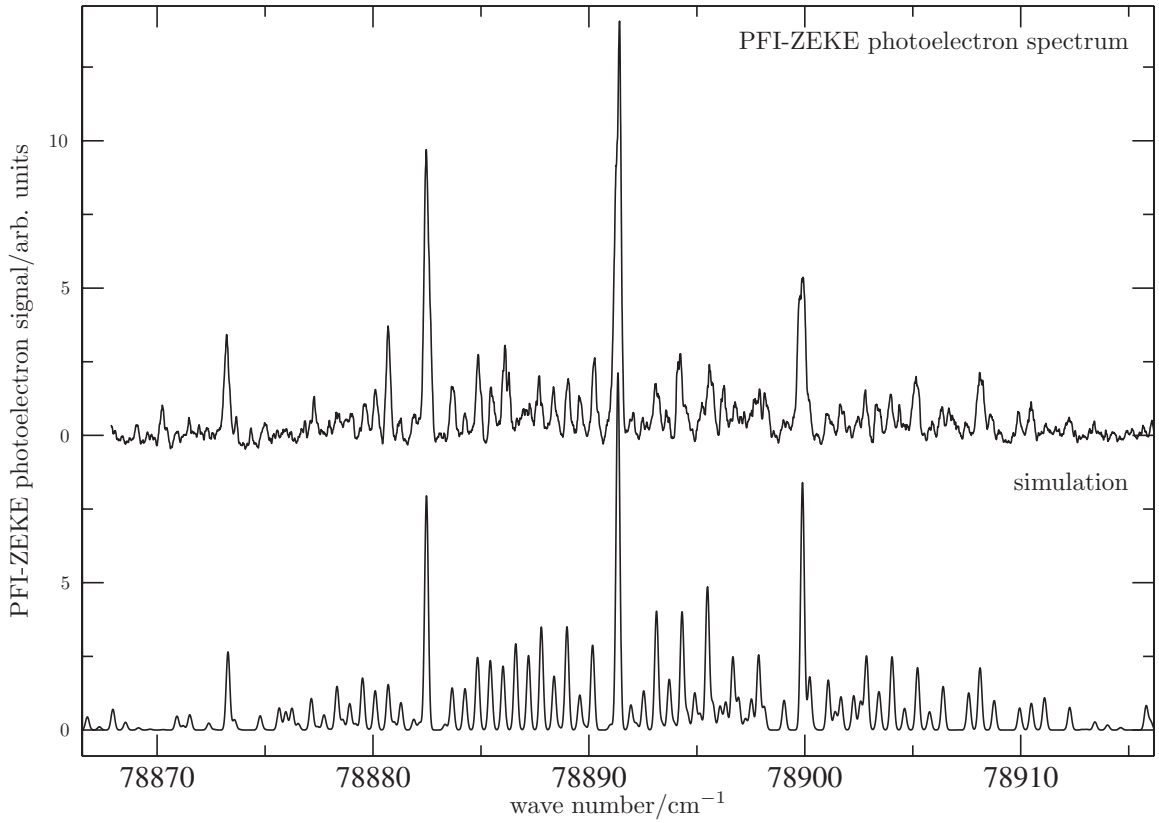

FIG. 5. Upper panel: PFI-ZEKE photoelectron spectrum of the $\tilde{X}^+\,{}^2E(4^1)\leftarrow\tilde{X}\,{}^1A_1(0^0)$ transition of C_3H_4. Lower panel: simulation using a Gaussian instrument function with a FWHM of 0.2 cm^{-1}.

partial wave because the $D_2(M)$ symmetry group does not contain any operations involving the inversion E^*, and the dipole moment representation is totally symmetric (A_1).

If the molecular cation is treated as being a prolate symmetric-top molecule of D_{2d} symmetry the rovibronic selection rules [Eq. (10)] can be expressed as

$$A_1 \leftrightarrow B_1, \quad A_2 \leftrightarrow B_2, \quad E \leftrightarrow E \tag{12}$$

for ℓ=even, and

$$A_1 \leftrightarrow A_1, \quad A_2 \leftrightarrow A_2, \quad E \leftrightarrow E \tag{13}$$

for ℓ=odd, which translates into $\Delta K = K^+ - K'' =$ odd for both even and odd photoelectron partial waves for the transitions $\tilde{X}^+\,{}^2E(0^0,\Gamma_{ve}^+=E)\leftarrow\tilde{X}\,{}^1A_1(0^0)$ and $\tilde{X}^+\,{}^2E(4^1,\Gamma_{ve}^+=E)\leftarrow\tilde{X}\,{}^1A_1(0^0)$. The selection rules in Eqs. (12) and (13) are of course compatible with those derived in Eq. (11) and differ only by the additional specification of the change in K_c. The fact that the selection rules derived in the $D_{2d}(M)$ molecular symmetry group are also insensitive to the parity of the partial wave of the outgoing electron results from the fact that the vibronic energy levels of the cation are doubly degenerate $(\Gamma_{ve}=E)$.

As expected for a prolate (near-prolate) symmetric-top molecule, the intensity distributions in the spectra displayed in Figs. 4 and 5 reveal a grouping of lines having the same ΔK (ΔK_a) values leading to characteristic $K'' \rightarrow K^+$ $(K_a'' \rightarrow K_a^+)$ branches for all possible values of $\Delta N = N^+ - N''$. The three strong peaks correspond to $\Delta N = 0$ "Q-type" branches. The assignment bars are only given for the origin band in Fig. 4 because the rotational structure and assignment of the 4^1 band are analogous. The assignment bars group transitions according to the same change in total angular momentum excluding spins $\Delta N = N^+ - N''$. The associated change in K (K_a) is indicated above each assignment bar in the notation $K'' \rightarrow K^+$ $(K_a'' \rightarrow K_a^+)$. Individual transitions are labeled according to the total angular momentum quantum number excluding spins N'' of the neutral ground state.

The analysis of the line positions of the photoelectron spectrum was carried out using the accurately known molecular constants for the neutral ground state.[35] Using either a rigid-rotor asymmetric-top Hamiltonian or a prolate symmetric-top Hamiltonian for the cationic state yielded equally satisfactory results. We present here the results obtained using the asymmetric-top Hamiltonian because the analysis of the vibronic structure presented in Sec. III clearly revealed the distortion of the cation along the torsional coordinate. Not surprisingly this analysis led to B^+ and C^+ rotational constants for the cationic states that are equal within the statistical uncertainties. The adiabatic ionization energy of C_3H_4, the fundamental torsional wave number and the rotational constants of $C_3H_4^+$ derived in a least-squares fitting procedure are summarized in Table III, which also contains molecular constants for $C_3D_4^+$ determined from the low-resolution spectrum displayed in Fig. 3(c). The experimental and calculated transition wave numbers of the origin band of the PFI-ZEKE photoelectron spectrum of allene are compared in Table IV. In this form, Table IV helps to assess the resolution that would be needed to resolve the K_c structure of

TABLE III. Ionization energies and rotational constants obtained from the PFI-ZEKE photoelectron spectrum of allene in a least-squares fit and used for the simulations of the rotational structure of the $\tilde{X}^+ {}^2E$ $(0^0,4^1) \leftarrow \tilde{X}$ bands of $C_3H_4^+$. Values in parentheses represent one standard deviation.

	$(E-E_{\text{neutral}})/hc$ (cm^{-1})	A (cm^{-1})	B (cm^{-1})	C (cm^{-1})
C_3H_4 neutral[a]	0.0(0)	4.811 655(11)	0.296 274 87(11)	0.296 274 87(11)
C_3D_4 neutral[b]	0.0(0)	2.4153(4)	0.232 13(3)	0.232 13(3)
$C_3H_4^+$ 0^0	78 142.92(50)[c]	4.696(18)	0.298(5)	0.287(5)
$C_3H_4^+$ 4^1	78 888.6(7)[c]	4.65(2)	0.296(5)	0.296(5)
$C_3D_4^+$ 0^0	78 248(2)[c]	2.32(5)	0.23213(3)[d]	0.23213(3)[d]

[a]Values taken from Ref. 35.
[b]Values taken from Ref. 43.
[c]Corrected for the field-induced shift.
[d]The B^+ and C^+ rotational constants of the cation were assumed to be equal to those of the neutral molecule when fitting the A^+ constant of $C_3D_4^+$.

specific lines. The assignments in Table IV can easily be converted into symmetric-top assignments by omitting the K_c^+ label because torsionally distorted allene is a near-prolate top and the K_a^+ quantum number is the good quantum number (K^+) in the limit of a symmetric top. The agreement between observed and calculated line positions is excellent, all deviations being less than 0.25 cm^{-1} (rms deviation of 0.07 cm^{-1}).

The orbital ionization model described in detail in Ref. 33 was used to calculate the rotational intensity distributions of the spectra. In the orbital ionization model, the angular momentum of the photon is assumed to be fully absorbed by the outgoing photoelectron, creating a hole of the same angular momentum composition as the molecular orbital out of which ionization occurs. The molecular orbital out of which ionization occurs in the $\tilde{X}^+ \leftarrow \tilde{X}$ photoionization transition of allene is schematically drawn in Fig. 6. This molecular orbital has only one nodal plane that contains the principal axis (a-axis) and the center of mass. Thus, the single-center expansion describing such a molecular orbital can only have contributions of atomiclike orbitals that conserve this nodal plane, i.e., atomiclike orbitals that have a quantum number $\lambda''=\pm 1$ for the projection of the angular momentum of the molecular orbital onto the principal axis ($z=a$-axis, see Fig. 6), which is denoted with the subscript π. For the simulations presented here which were carried out using Eq. (7) of Ref. 33, only contributions to the single-center expansion of p_π and d_π angular momentum character have been taken into account with relative weights of 0.6 and 1.0, respectively, which implies the selection rules $|\Delta N|=|N^+-N''|\leq 2$ and $\Delta K_a=K_a^+-K''=\pm 1$.

The simulated spectra presented in Figs. 4 and 5 capture the main features of the experimental spectra and reproduce the relative intensities of the transitions almost quantitatively. A rotational temperature of 10 K was assumed in the simulations and only ground state levels with $N''\leq 8$ and $K''\leq 2$ contribute significantly to the spectrum. At this low rotational temperature, the centrifugal and higher-order rotational terms in the rotational Hamiltonian can be neglected at our experimental resolution.

A careful comparison of the spectra of the origin and the 4^1 bands reveals that the lines of the latter spectrum are slightly but unambiguously broader (FWHM=0.2 cm^{-1}) than those of the former (FWHM=0.15 cm^{-1}). The fact that the rotational lines appear broader in the 4^1 band than in the 0^0 band may be an indication of large-amplitude motions, which cannot be explained with the vibronic model presented in Sec. III, as will be discussed in Sec. V.

V. THE ROTATIONAL STRUCTURE OF THE 4^2 AND 4^3 BANDS

Figure 7 compares the PFI-ZEKE photoelectron spectra of the 0^0, 4^1, 4^2, and 4^3 bands of C_3H_4 recorded with both laser systems. As discussed in Sec. IV, the rotational structures of the 0^0 and 4^1 bands are qualitatively very similar and are dominated by the three strong Q-type branches. The rotational structures of the 4^2 and 4^3 bands, however, do not exhibit this pattern and appear strongly perturbed.

In the rotational structure of the 4^2 band, the central three "Q-type-branch" features appear doubled with a separation of $\simeq 1$ cm^{-1}. By comparison to the assignment of the rotational structure analyzed for the 0^0 and 4^1 bands, the strong double peak at 79 600 cm^{-1} would then correspond to Q-type transitions of $K_a^+=0 \leftarrow K''=1$ character. An a-type Coriolis interaction cannot shift levels of rotational quantum number $K_a=0$ so that two distinct vibrational states separated by 1 cm^{-1} may lie in this energy region. Beside the slight broadening of the transitions in the spectrum of the 4^1 level (see Sec. IV), the doubling of the Q-type transitions mentioned above is a second indication of a possible effect of large-amplitude motions. As stated in Sec. III, no such splittings result from the Hamiltonian of Eq. (2). Such a splitting may result from a tunneling motion through the D_{2h} barrier along the torsional coordinate at $\tau=0°$, as observed in $C_2H_4^+$.[36] The extension of the treatment of the JT effect in $C_3H_4^+$ to include this tunneling motion would be desirable, and progress in this direction will be reported in a separate publication. Alternatively, the irregular rotational structure of the 4^2 and 4^3 levels may also indicate heterogeneous rovibronic perturbations along the a-axis of the system, such as a perturbation resulting from an a-type Coriolis interaction, or higher-order rovibrational perturbations.

In addition to the perturbations in the rotational structures of 4^2 and 4^3 bands of the PFI-ZEKE photoelectron

TABLE IV. Observed and calculated line positions (in cm^{-1}) of the PFI-ZEKE photoelectron spectrum of the origin band of the $\tilde{X}^+\,^2E\ (0^0) \leftarrow \tilde{X}\,^1A_1(0^0)$ transition of C_3H_4.

$N''_{K''}$	$N^+_{K_a^+K_c^+}$	$\tilde{\nu}_{\mathrm{expt}}$	$\tilde{\nu}_{\mathrm{calc}}$
7_1	5_{05}	78 129.01	78 128.99
6_1	4_{04}	78 130.26	78 130.21
5_1	3_{03}	78 131.42	78 131.43
8_1	7_{07}	78 131.87	78 131.85
7_1	6_{06}	78 132.61	78 132.50
4_1	2_{02}		78 132.63
6_1	5_{05}	78 133.14	78 133.14
5_1	4_{04}	78 133.80	78 133.77
3_1	1_{01}		78 133.83
4_1	3_{03}	78 134.38	78 134.39
3_1	2_{02}	78 135.01	78 135.00
2_1	0_{00}		78 135.03
2_1	1_{01}	78 135.59	78 135.61
1_1	0_{00}	78 136.19	78 136.21
8_1	8_{08}	78 136.75	78 136.53
7_1	7_{07}		78 136.59
6_1	6_{06}		78 136.64
5_1	5_{05}		78 136.69
4_1	4_{04}		78 136.73
3_1	3_{03}		78 136.76
2_1	2_{02}		78 136.78
1_1	1_{01}		78 136.80
1_1	2_{02}	78 137.99	78 137.97
7_0	5_{14}		78 137.99
2_1	3_{03}	78 138.54	78 138.54
3_1	4_{04}	78 139.18	78 139.10
6_0	4_{13}		78 139.21
4_1	5_{05}	78 139.68	78 139.65
1_1	3_{03}		78 139.72
5_1	6_{06}	78 140.39	78 140.20
5_0	3_{12}		78 140.38
8_0	7_{17}	78 140.64	78 140.62
6_1	7_{07}		78 140.74
2_1	4_{04}	78 140.88	78 140.88
7_0	6_{16}	78 141.31	78 141.30
7_1	8_{08}		78 141.27
4_0	2_{11}	78 141.56	78 141.57
6_0	5_{15}	78 141.99	78 141.97
3_1	5_{05}		78 142.02
5_0	4_{14}	78 142.70	78 142.63
3_0	1_{10}		78 142.76
4_1	6_{06}	78 143.25	78 143.16
4_0	3_{13}		78 143.28
3_0	2_{12}	78 143.86	78 143.90
5_1	7_{07}	78 144.30	78 144.29
2_0	1_{11}	78 144.53	78 144.53
6_1	8_{08}	78 145.48	78 145.42
8_0	8_{17}	78 145.71	78 145.65
7_0	7_{16}		78 145.66
6_0	6_{15}		78 145.68
5_0	5_{14}		78 145.69
4_0	4_{13}		78 145.70
3_0	3_{12}		78 145.71
2_0	2_{11}		78 145.71
1_0	1_{10}		78 145.72
0_0	1_{11}	78 146.30	78 146.30
7_1	9_{09}		78 146.53
1_0	2_{12}	78 146.87	78 146.87
2_0	3_{13}	78 147.44	78 147.42
0_0	2_{11}		78 147.50
3_0	4_{14}	78 147.96	78 147.96
4_0	5_{15}	78 148.50	78 148.49
1_0	3_{12}		78 148.67
5_0	6_{16}	78 149.01	78 149.00
6_0	7_{17}	78 149.52	78 149.51
2_0	4_{13}	78 149.89	78 149.85
7_0	8_{18}		78 149.99
8_0	9_{19}	78 150.44	78 150.47
6_1	5_{24}, 5_{23}		78 150.75
3_0	5_{14}	78 150.97	78 151.02
5_1	4_{23}, 4_{22}	78 151.49	78 151.38
4_1	3_{21}, 3_{22}		78 152.00
4_0	6_{15}	78 152.23	78 152.20
3_1	2_{21}, 2_{20}	78 152.66	78 152.62
5_0	7_{16}	78 153.42	78 153.37
7_1	7_{26}, 7_{25}	78 154.45	78 154.21
6_1	6_{25}, 6_{24}		78 154.26
5_1	5_{24}, 5_{23}		78 154.31
4_1	4_{23}, 4_{22}		78 154.34
3_1	3_{22}, 3_{21}		78 154.37
2_1	2_{21}, 2_{20}		78 154.40
6_0	8_{17}		78 154.54
1_1	2_{21}, 2_{20}	78 155.68	78 155.58
2_1	3_{22}, 3_{21}	78 156.15	78 156.15
3_1	4_{23}, 4_{22}	78 156.82	78 156.71
4_1	5_{24}, 5_{23}	78 157.39	78 157.27
1_1	3_{22}, 3_{21}		78 157.34
5_1	6_{25}, 6_{24}	78 157.91	78 157.82
6_1	7_{26}, 7_{25}		78 158.35
2_1	4_{23}, 4_{22}	78 158.58	78 158.49
7_1	8_{27}, 8_{26}		78 158.89
3_1	5_{24}, 5_{23}	78 159.73	78 159.64
4_1	6_{24}, 6_{25}	78 160.92	78 160.78
5_1	7_{26}, 7_{25}		78 161.91
8_2	8_{36}, 8_{35}	78 162.69	78 162.62
7_2	7_{35}, 7_{34}		78 162.68
6_2	6_{34}, 6_{33}		78 162.73
5_2	5_{33}, 5_{32}		78 162.78
4_2	4_{32}, 4_{31}		78 162.81
3_2	3_{31}, 3_{30}		78 162.84

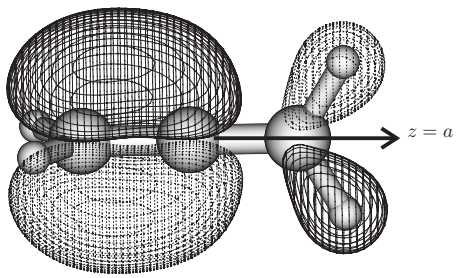

FIG. 6. Schematic diagram of the highest occupied molecular orbital of neutral allene out of which ionization occurs in the $\tilde{X}^+\,^2E \leftarrow \tilde{X}\,^1A_1$ transition. The image was generated using the MOLDEN software package (Ref. 37) with the input from a Hartree–Fock calculation using the MOLPRO software package (Ref. 38). The different shadings of the lobes indicate opposite phases of the orbital.

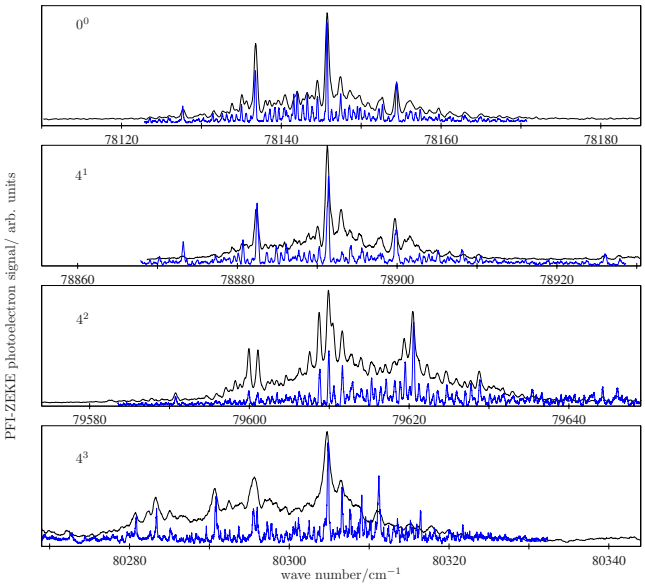

FIG. 7. (Color online) Comparison of the rotational structure of the first four torsional bands in the photoelectron spectrum of the $\tilde{X}^+ \leftarrow \tilde{X}$ transition of C_3H_4. In each panel, the upper (lower) trace was recorded with the low- (high-) resolution vuv laser system.

spectra of C_3H_4 visible in Fig. 7, seven less intense bands, labeled I–VII, are observed in their vicinity, as illustrated in more detail in Figs. 8(a) and 8(b). The positions of these vibronic bands relative to the adiabatic ionization threshold of allene are summarized in Table II. Surprisingly, no bands of comparable intensity near the strong bands belonging to the progression in the torsional mode are observed in the PFI-ZEKE photoelectron spectra of allene-d_4 (see Fig. 3). The stick spectrum obtained from the vibronic calculations performed on the basis of Eq. (2) (see Sec. III) is also shown in Fig. 8 and only reveals two bands in each of the spectral regions. The linear JT effect as described in Sec. III can thus

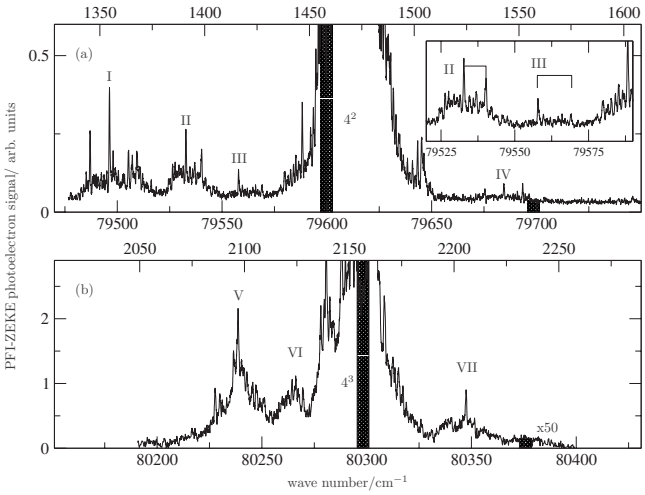

FIG. 8. Enlarged view of the PFI-ZEKE photoelectron spectra in the region of (a) the 4^2 and (b) the 4^3 bands of the $\tilde{X}^+ \leftarrow \tilde{X}$ transition of C_3H_4. Seven bands of relatively low intensity labeled I–VII are visible. Bars indicate the position and relative intensity of the ν_4 and ν_6 modes calculated with the JT Hamiltonian in Eq. (2). The inset in (a) shows an enlarged view of bands II and III and indicates the separation of the two Q-type branches observed in each of them. The upper horizontal scale corresponds to the internal energy of the cation.

TABLE V. Overview of the vibrational states that could contribute to the PFI- ZEKE photoelectron spectrum of allene in the vicinity of the 4^2 level of $C_3H_4^+$. The wave numbers $\tilde{\nu}_{i,H}^{neutral}$ have been calculated using the harmonic wave numbers of neutral C_3H_4. The vibrational symmetry of each band is given in the third column.

$\tilde{\nu}_{i,H}^{neutral}$ (cm^{-1})	ν_i	Vibrational symmetry
1188.8[a]	11^1+10^1	$a_1+a_2+b_1+b_2$
1351.7[a]	11^1+9^1	$a_1+a_2+b_1+b_2$
1395.0[b]	7^1	b_2
1393.4[a]	11^4	$2(a_1+a_2+b_1+b_2)$
1443.3[a]	2^1	a_1
1683.1[a]	10^2	$a_1+a_2+b_1+b_2$
1697.4[a]	4^2	a_1
1920.2[c]	6^1	b_2
1920.8[b]	3^1+4^1	b_1

[a]Reference 44 and references therein.
[b]Reference 43 and references therein.
[c]Reference 41.

not be the reason for the large number of weak bands observed. Table V summarizes the vibrational states that could contribute to the PFI-ZEKE photoelectron spectrum of allene in the energy region from 1100 to 2000 cm^{-1} above the origin based on the harmonic wave numbers of neutral allene, which we assume are similar to those of $C_3H_4^+$. Of the nine bands, the 11^4 and 3^1+4^1 bands are unlikely because neither the 11^2 nor the 3^1 bands are observed in the spectra, although they both are totally symmetric and allowed by symmetry. A weak transition to the fundamental of the JT active mode ν_6 is expected from the vibronic calculations in the vicinity of band IV, 1543 cm^{-1} above the origin and the calculated intensity roughly matches the experimental observation.

All bands in the vicinity of the 4^2 band in Fig. 8(a) reveal sharp rotational features, whereas sharp rotational structures are hardly present in the vicinity of the 4^3 band [see Fig. 8(b)]. The sharp features in bands I–IV can be interpreted as clusters of Q-type transitions as observed in the rotational structure of the origin band (0^0) and first fundamental torsional band (4^1). Band I has a rotational structure with two strong lines spaced by ≈9.2 cm^{-1}. Bands II and III [see inset of Fig. 8(a)] also show sharp rotational structures, with the two sharp peaks of band II being separated by ≈7.6 cm^{-1}, and those of band III by ≈11.3 cm^{-1}. A possible explanation of these wave number intervals between what we tentatively assign as Q-type branches in the rotational structure of bands II and III could be an a-type Coriolis coupling, which would reduce the spacing in the lower and increase it in the upper band.[31]

The rotational structure of the 4^3 band is even more complex and perturbed than that of the 4^2 band and no regular spacing between Q-type-branch features can be discerned. The density of states is already high 2000 cm^{-1} above the origin with more than 18 vibrational levels expected in the vicinity (±150 cm^{-1}) of the strong 4^3 band. A polyad of many interacting bands is the likely origin of the complicated rotational structures and of the observation of the bands I–VII in Fig. 8. Band VII may correspond to the 4^16^1 combination band. However, the calculated intensity is

much weaker than that of band VII. Information from *ab initio* quantum chemical calculations would be desirable to advance the current understanding of this spectral region.

Vibronic calculations that solely include the JT active modes ν_4 and ν_6, although adequate to describe the positions and intensities of the strong bands 4^2 and 4^3, clearly fail to account for the details of the (ro-)vibronic structure and do not provide an explanation for the perturbed rotational structure and the weak satellite bands. Most current theoretical treatments of the vibronic structure of molecules undergoing the JT effect concentrate on a very limited number of strongly JT active modes.[29,11] The present results point at a need to extend the theoretical treatment to include a more complete set of interactions such as Fermi interactions, Coriolis interactions, and interactions resulting from the bilinear coupling terms of the JT Hamiltonian which are often ignored. Obtaining such a set of parameters may necessitate extensive *ab initio* calculations.

VI. CONCLUSIONS

The present investigation of the JT effect in the $\tilde{X}^+\,^2E$ ground state of the allene cation has enabled the derivation of the first adiabatic ionization energy of allene and the determination of a set of molecular constants: rotational constants describing the lowest two torsional levels and JT coupling constants describing the overall vibronic structure of the photoelectron spectra.

The high-resolution photoelectron spectra reveal complex spectral structures arising from perturbations not included in the standard treatment of the $E \otimes (b_1 \oplus b_2)$ JT effect in Eq. (2), which neglects anharmonic and Coriolis interactions and bilinear JT couplings on the one hand and disregards the possibility of large-amplitude motion through planar structures on the other. In future, a complete treatment of the (ro-)vibronic interactions (Coriolis interactions, bilinear JT coupling and higher-order vibrational interactions and large-amplitude motion through planar structures) in $C_3H_4^+$ and other molecules of similar complexity using *ab initio* quantum chemical calculations would be desirable.

ACKNOWLEDGMENTS

We thank G. Grassi (ETH Zurich) for the synthesis C_3H_4, and Dr. U. Hollenstein (ETH Zurich) for experimental help. We also thank Professor S. Willitsch (Basel) and Dr. H. J. Wörner (NRC Ottawa) for useful discussions. This work was supported financially by the Swiss National Science Foundation under project No. 200020-116245 and the ETH Zurich.

[1] A. Coustenis, Th. Encrenaz, B. Bézard, G. Bjoraker, G. Graner, M. Dang-Nhu, and E. Arié, Icarus **102**, 240 (1993).
[2] A. Coustenis, B. Bézard, and D. Gautier, Icarus **80**, 54 (1989).
[3] A. Coustenis, A. Salama, B. Schulz, S. Ott, E. Lellouch, Th. Encrenaz, D. Gautier, and H. Feuchtgruber, Icarus **161**, 383 (2003).
[4] X. Song, Y. Bao, R. S. Urdahl, J. N. Gosine, and W. M. Jackson, Chem. Phys. Lett. **217**, 216 (1994).
[5] R. H. Qadiri, E. J. Feltham, E. E. H. Cottrill, N. Taniguchi, and M. N. R. Ashfold, J. Chem. Phys. **116**, 906 (2002).
[6] R. H. Qadiri, E. J. Feltham, N. H. Nahler, R. P. García, and M. N. R. Ashfold, J. Chem. Phys. **119**, 12842 (2003).
[7] S. Harich, Y. T. Lee, and X. Yang, Phys. Chem. Chem. Phys. **2**, 1187 (2000).
[8] A. M. Mebel, W. M. Jackson, A. H. H. Chang, and S. H. Lin, J. Am. Chem. Soc. **120**, 5751 (1998).
[9] D. Stranges, M. Stemmler, X. Yang, J. D. Chesko, A. G. Suits, and Y. T. Lee, J. Chem. Phys. **109**, 5372 (1998).
[10] H. A. Jahn and E. Teller, Proc. R. Soc. London, Ser. A **161**, 220 (1937).
[11] I. B. Bersuker, *The Jahn-Teller Effect* (Cambridge University Press, Cambridge, 2006).
[12] C. Baker and D. W. Turner, J. Chem. Soc. D **9**, 480 (1969).
[13] J. W. Rabalais, T. Bergmark, L. O. Werme, L. Karlsson, and K. Siegbahn, Phys. Scr. **3**, 13 (1971).
[14] A. A. Iverson and B. R. Russell, Spectrochim. Acta, Part A **28**, 447 (1972).
[15] R. K. Thomas and H. Thompson, Proc. R. Soc. London, Ser. A **339**, 29 (1974).
[16] Z. Z. Yang, L. S. Wang, Y. T. Lee, D. A. Shirley, S. Y. Huang, and W. A. Lester, Jr., Chem. Phys. Lett. **171**, 9 (1990).
[17] P. Baltzer, B. Wannberg, M. Lundqvist, L. Karlsson, D. M. P. Holland, M. A. MacDonald, and W. von Niessen, Chem. Phys. **196**, 551 (1995).
[18] L. S. Cederbaum, W. Domcke, and H. Köppel, Chem. Phys. **33**, 319 (1978).
[19] C. Woywod and W. Domcke, Chem. Phys. **162**, 349 (1992).
[20] R. Signorell, H. Palm, and F. Merkt, J. Chem. Phys. **106**, 6523 (1997).
[21] U. Hollenstein, H. Palm, and F. Merkt, Rev. Sci. Instrum. **71**, 4023 (2000).
[22] C. E. Moore, *Atomic Energy Levels*, Natl. Bur. Stand. (U.S.) Circ. No. 467/2 (U.S. GPO, Washington, D. C., 1952).
[23] T. Trickl, M. J. J. Vrakking, E. Cromwell, Y. T. Lee, and A. H. Kung, Phys. Rev. A **39**, 2948 (1989).
[24] S. Willitsch, Ch. Jungen, and F. Merkt, J. Chem. Phys. **124**, 204312 (2006).
[25] A. T. Morse and L. C. Leitch, J. Org. Chem. **23**, 990 (1958).
[26] U. Hollenstein, R. Seiler, H. Schmutz, M. Andrist, and F. Merkt, J. Chem. Phys. **115**, 5461 (2001).
[27] U. Hollenstein, R. Seiler, A. Osterwalder, M. Sommavilla, A. Wüest, P. Rupper, S. Willitsch, G. M. Greetham, B. Brupbacher-Gatehouse, and F. Merkt, Chimia **55**, 759 (2001).
[28] T. A. Barckholtz and T. A. Miller, Int. Rev. Phys. Chem. **17**, 435 (1998).
[29] I. B. Bersuker, Chem. Rev. (Washington, D.C.) **101**, 1067 (2001).
[30] A. D. O. Bawagan, T. K. Ghanty, E. R. Davidson, and K. H. Tan, Chem. Phys. Lett. **287**, 61 (1998).
[31] G. Herzberg, *Molecular Spectra and Molecular Structure*, Vol. II, Infrared and Raman Spectra of Polyatomic Molecules (Krieger, Malabar, 1991).
[32] R. Signorell and F. Merkt, Mol. Phys. **92**, 793 (1997).
[33] S. Willitsch and F. Merkt, Int. J. Mass Spectrom. **245**, 14 (2005).
[34] P. R. Bunker and P. Jensen, *Molecular Symmetry and Spectroscopy*, 2nd ed. (NRC Research, Ottawa, 1998).
[35] F. Hegelund, N. Andresen, and M. Koivusaari, J. Mol. Spectrosc. **149**, 305 (1991).
[36] S. Willitsch, U. Hollenstein, and F. Merkt, J. Chem. Phys. **120**, 1761 (2004).
[37] G. Schaftenaar and J. Noordik, J. Comput.-Aided Mol. Des. **14**, 123 (2000).
[38] H.-J. Werner, P. J. Knowles, R. Lindh *et al.*, MOLPRO, version 2002.6, a package of *ab initio* programs, 2002.
[39] F. Hegelund and H. B. Andersen, J. Raman Spectrosc. **3**, 73 (1975).
[40] H. B. Andersen, F. Hegelund, N. R. Zangenberg, and F. Winther, J. Raman Spectrosc. **6**, 238 (1977).
[41] J. Plíva, K. Rousan, and S. R. Polo, J. Mol. Spectrosc. **101**, 395 (1983).
[42] J. Plíva and C. A. Martin, J. Mol. Spectrosc. **91**, 218 (1982).
[43] F. Hegelund, J. L. Duncan, and D. C. McKean, J. Mol. Spectrosc. **65**, 366 (1977).
[44] W. Knippers, K. Van Helvoort, M. De Felici, J. Reuss, and S. Stolte, Chem. Phys. **105**, 27 (1986).